Journal of
Materials Chemistry A

ROYAL SOCIETY
OF CHEMISTRY

PAPER

View Article Online
View Journal

Check for updates

Cite this: DOI: 10.1039/d6ta01920j

The spin thermoelectric effect in nonmagnetic chiral materials

Sheli Muzafe Reiss,[a] Clement Gedeon,†[bc] Ohad Golan,[a] Ofek Vardi,[ag] Dror Merhav, [a] Christos L. Chochos, ‡[b] Shira Yochelis, [a] David H. Waldeck, [d] Jonas Fransson,[e] Jeanne Crassous, *[c] Ron Naaman *[f] and Yossi Paltiel *[a]

Received 4th March 2026
Accepted 18th May 2026

DOI: 10.1039/d6ta01920j

rsc.li/materials-a

p–n junctions are commonly applied in thermoelectric cooling devices based on the Peltier effect. Here the effect of chirality on the thermoelectric properties of p–n junction devices was studied by inserting a chiral polymer at the interface between p- and n-silicon. Although the chiral polymer covered only part of the interface, it increased the temperature gradient between the two parts of the device by about a factor of two compared with p–n junctions in which the chiral polymer was replaced by achiral molecules or a racemic mixture of the polymer. The contact heating was about the same for all cases, the devices with the chiral polymer layer displayed a large additional thermal gradient. The increase in the thermal gradient can be rationalized in terms of the chiral-induced spin selectivity effect, *i.e.*, the spin dependence of conduction through the chiral material and therefore a reduction of entropy through spin orientation. Considering that a subset of the current is conducted through the chiral molecules, the results indicate that the chiral thermal effect is much more efficient than the Peltier effect. The experimental results are followed by a phenomenological model as well as a theoretical explanation.

Introduction

The need for faster and more powerful computers is driving the need for thermal cooling solutions that operate at the micron and submicron scale.[1] This need also exists for many other devices ranging from optoelectronic devices such as laser diodes, RF, and microwave devices, to other electronic devices such as memory devices. Hence, there is demand for thermal management technologies that will improve the efficiency of current thermoelectric devices. At present, most thermoelectric cooling devices are based on the Peltier effect, which was discovered more than a century ago.[2]

The Peltier effect enables compact, solid-state thermoelectric cooling; however, its widespread adoption remains limited by its relatively low efficiency.[3] Regarding the Peltier effect, several features can limit its efficiency. The temperature difference between the cold and warm side should be small for a single device; therefore, multi-stage Peltier elements are used when higher temperature differences are needed. In addition, an efficient Peltier element requires two, often incompatible, properties. Moreover, the thermoelectric material should have a low thermal conductivity that preserves the generated heat gradient, while at the same time have high electrical conductivity. Because both of these properties are affected by electron mobility, this requirement limits the efficiency of the device. This issue is typically solved by using exotic materials or semiconductor pellets fabricated from n-type and p-type bismuth telluride,[4] and recently from organic polymers.[5,6] The efficiency of Peltier-based devices is only about 10–15% of that from an ideal Carnot cycle, compared with the 40–60% achieved by conventional compression-cycle systems.[7]

In recent years intensive research has been performed to explore the ability to utilize the electron spin in thermoelectric devices.[8,9] Typically, such devices use a magnetic material as the spin source, or for converting the heat to spins.[10–16] In another study, chiral phonons were found to activate the spin current as the result of a temperature gradient.[17] Here the magnetization is induced before the cooling effect and the cooling does not use the reduction of entropy associated with the magnetization. Therefore, these devices are usually similar in efficiency to

---

[a] Applied Physics Department, Center for Nano-Science and Nano-Technology, The Hebrew University of Jerusalem, Jerusalem 9190401, Israel. E-mail: paltiel@mail.huji.ac.il

[b] Advent Technologies SA, Stadiou Str, Platani 26504, Patras, Greece

[c] Univ Rennes, CNRS, ISCR – UMR 6226, 35000 Rennes, France

[d] Department of Chemistry, University of Pittsburgh, Pittsburgh, Pennsylvania 15260, USA

[e] Department of Physics and Astronomy, Uppsala University, Box 516, Uppsala, 751 21, Sweden

[f] Department of Chemical and Biological Physics, Weizmann Institute, Rehovot 7610001, Israel

[g] The Racah Institute of Physics, The Hebrew University of Jerusalem, Jerusalem 91904, Israel

† Current address: LCPO Bordeaux, CNRS – UMR 5629, 33615 Pessac, France.

‡ Current address: Institute of Chemical Biology National Hellenic Research Foundation, Athens 11635, Greece.

standard Peltier devices. In contrast, the magnetothermal effect[18,19] pumps heat *via* magnetization and the demagnetization of ferromagnets. This process is based on spin alignment, during the magnetization process, which results in the release of heat to the environment, and heat pumping from the environment upon spin randomization, namely, demagnetization. Magneto-cooling processes usually require bulky magnets; however, this technique is not applicable for cooling small devices or localized areas on an electrical circuit. Previous studies utilizing chiral materials on ferromagnetic surfaces showed that they have profound magnetic properties.[20]

Chiral systems display spin-polarized charge current through the chiral-induced spin selectivity (CISS) effect, which preferentially transmits electrons of a specific spin orientation for a given enantiomer.[21] This spin-dependent transport can be used for reducing electron entropy by orienting spins in the chiral material and emitting the heat at one side of the system. After passing through the chiral system, the spins lose their alignment and the electrons' entropy increases; as a result, the temperature of the current collector is reduced. Hence, the chiral system can be used as a thermoelectric device that acts similarly to a magnetothermal system, but with no need for a bulky magnet. Here the effects of spin alignment and randomization are attributed to the increase and reduction in the entropy of the environment, respectively. This effect exists for the chiral system in addition to the Peltier effect. The experiments shown here reveal that the efficiency of the chiral thermoelectric effect can significantly exceed that of the Peltier effect.

In this study, we demonstrate the efficiency of this new effect that arises from CISS in a thermoelectric device based on a horizontal silicon p–n junction, which is fabricated by integrating the chiral polymer IDT6-Hel recently reported by some of us.[22] Note that spin polarization is expected using the chiral polymer, even without fully utilizing the polymer.[23] The device is designed to operate as a solid-state cooling device with enhanced heat pumping efficiency and an improved coefficient of performance (COP).

Experimental methods

The solid-state device is based on a lateral silicon p–n junction, doped with boron (p-type) and phosphorus (n-type) that was fabricated using standard photolithography and p-type silicon ion implantation (produced by IBS company, France; Fig. 1a). The ion was implanted using four different cascading energies, generating precise and uniform doping to a 200 nm depth (see Fig. S1 in the SI). The junction dimensions are 100 μm × 100 μm with a depth of 200 nm. At the p–n interface, a nanoscale slit (3 μm wide, 100 nm deep) was introduced by focused ion beam (FIB) milling (see Fig. S2 in the SI). Fig. 1a(ii) displays a thermal image of the junction taken from above while current is flowing in the device. To investigate the influence of chirality on the thermal properties of the junction, the slit was subsequently filled with either a racemic mixture or an enantiopure *P*- and *M*-IDT6-Hel polymer (Fig. 1b).

Next, we will also use IDT-P and IDT-M for the *P*- and *M*-IDT6-Hel polymers. The polymer consists of oligomers comprising alternating indacenodithiophene and carbo[6]helicene units, synthesized in racemic, *P*, and *M* enantiomeric forms (Fig. 1b). For thermal measurements, the temperatures of the p and n sides were monitored using an infrared (IR) thermal camera with 0.1 K thermal resolution (Fig. 1a(ii)), while applying DC current. The material was prepared using previously reported procedures;[24] the number of the average molecular weights ($\overline{M_n}$) of 3.5–6.3 kg mol^{-1} is shown. Note that nearly the same low electrical conductivity was measured for the enantiopure and racemic polymer incorporating 1% and 11% of the helicenic units. It is thus expected that both enantiomers of IDT6-Hel incorporating 50% of helicene have similarly low conductivity, as well as in the racemic polymer, probably due to domain forming and partial spin filtering.

The enantiomeric forms display strong, mirror-image electronic circular dichroism responses over the 250 and 550 nm range, with $\Delta\varepsilon$ values of up to ±525 M^{-1} cm^{-1} in CH_2Cl_2 solutions (Fig. 1c).

The chiral polymer was introduced into the device by drop-casting a polymer solution onto the p–n junction. Upon solvent evaporation, a thin polymer layer filled the slit and its immediate surroundings, establishing direct contact with the silicon junction. The polymer could be subsequently removed by rinsing with the deposition solvent, allowing sequential measurements on the same device. This approach enabled the deposition, removal, and redeposition of different polymer variants, ensuring repeatable and controlled comparisons under identical device conditions. We compared the results on the same device using a systematic procedure, *e.g.*, blank, chiral polymer, achiral polymer, and blank (without polymers), as well as randomly varied measurements.

In this work we show that placing the enantiopure chiral polymer in the device slit while driving current changes the temperature gradient and the total heating dramatically, compared with cases using achiral material and racemic mixtures of the polymer.

Results

To evaluate the device performance, we performed both electrical and thermal characterizations. Current–voltage (*IV*) measurements were recorded to verify the diode behavior for the p–polymer–n device element and to evaluate the interface resistance. Thermal measurements were conducted using an infrared camera (IR; Optris Xi 400) to quantify the temperature difference across the junction under varying current bias conditions. A schematic illustration of the measurement system is presented in Fig. 1a.

For quantifying the spin-polarized electron transport through the chiral enantiopure IDT-P and IDT-M polymers, the magnetoresistance was measured using magnetic conducting AFM on spin-coated films of the polymer on an Au electrode. Typical results are presented in Fig. 2 for IDT-M. Spin polarization was defined by measuring the current with the tip magnetized either north or south. The magnetoresistance is

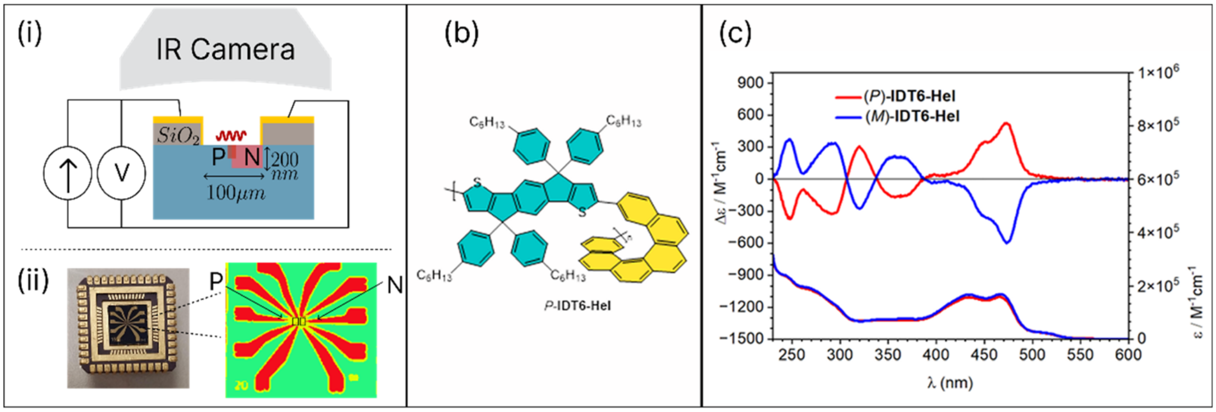

Fig. 1 (a) Scheme (i) illustrates the thermal measurement setup and device structure as a sideview. The polymer height of 20 nm above the slit was measured by AFM (see SI Fig. S3). Scheme (ii) shows a thermal image of the device and an optical image, from the top. The slit is in the center of the picture. The temperature is recorded over time using a thermal camera, measuring predefined measurement areas. Red denotes hot and green denotes cold (repeated thermal measurements are shown in SI Fig. S5). The resolution of the thermal measurements is 0.1 K, using an Optris Xi 400 camera; the same device was measured with and without the polymers. The measured areas are 200 × 400 μm; thus, it includes the contacts area. (b) Chemical structure of the chiral oligomer (the P isomer is shown) inserted into the p–n junction. (c) Electronic circular dichroism (top part) and UV-vis absorption spectra (bottom part) are shown for (*P*)/(*M*)-IDT6-Hel oligomers in CH_2Cl_2 measured at 25 °C.

quantified by MR = $(I_S - I_N)/(I_S + I_N)$, where I_S and I_N are the currents when the tip is magnetized south or north, respectively. The inset of Fig. 2 shows the calculated spin polarization for 10 nm-thick spin-coated IDT-P and IDT-M polymers. For both enantiomers, the spin polarization exceeds 70% in certain voltage regimes.

An infrared camera was used to measure the temperature gradients and changes. The temperature increase is reported relative to the baseline temperature measured at zero electrical current. To ensure steady-state conditions, temperatures were recorded for 15 seconds following a 165 second stabilization period, after each current step. The temperature is measured for different current steps. The device voltage was simultaneously measured, and the electrical power was calculated to generate plots of the temperature difference as a function of power (Fig. 3a and b).

Measurements were performed under three p–polymer–n junction conditions: without polymer deposition (WO), with

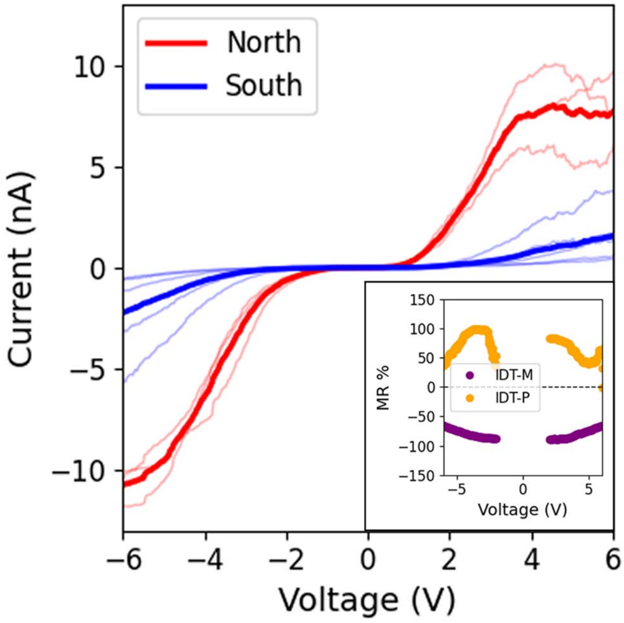

Fig. 2 Spin polarization is quantified by MR = $(I_S - I_N)/(I_S + I_N)$, where I_S is the current intensity for south magnetization, whereas I_N represents the current intensity for north magnetization of the tip. (Inset) Calculated spin polarization for both enantiomers. IDT-P seems to have pinholes that conduct at voltages above 6 V.

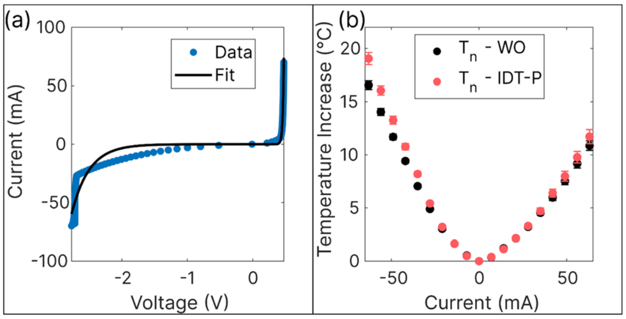

Fig. 3 (a) Current as a function of voltage for the bare p–n junction device element without polymer. The black line denotes a fit to an idealized p–n junction. Note that the diode is not perfect and some leakage current is expected due to the implantation profile (b) plots of the temperature increase *vs.* current on the n-side of the junction, T_n, are shown for the p–n junction device without polymer (WO) and for a device with the chiral polymer IDT-Hel-P-50. A larger temperature difference for forward and backward currents is observed for the device with a chiral polymer. For these data the same device was used for measurements, and the polymer was added and cleaned 5 times on several devices to compare the results (extended data for the IDT-P and IDT-Racemic devices can be seen in SI Fig. S4). In some devices current can flow around the implanted area; it adds a small leakage current for reverse bias.

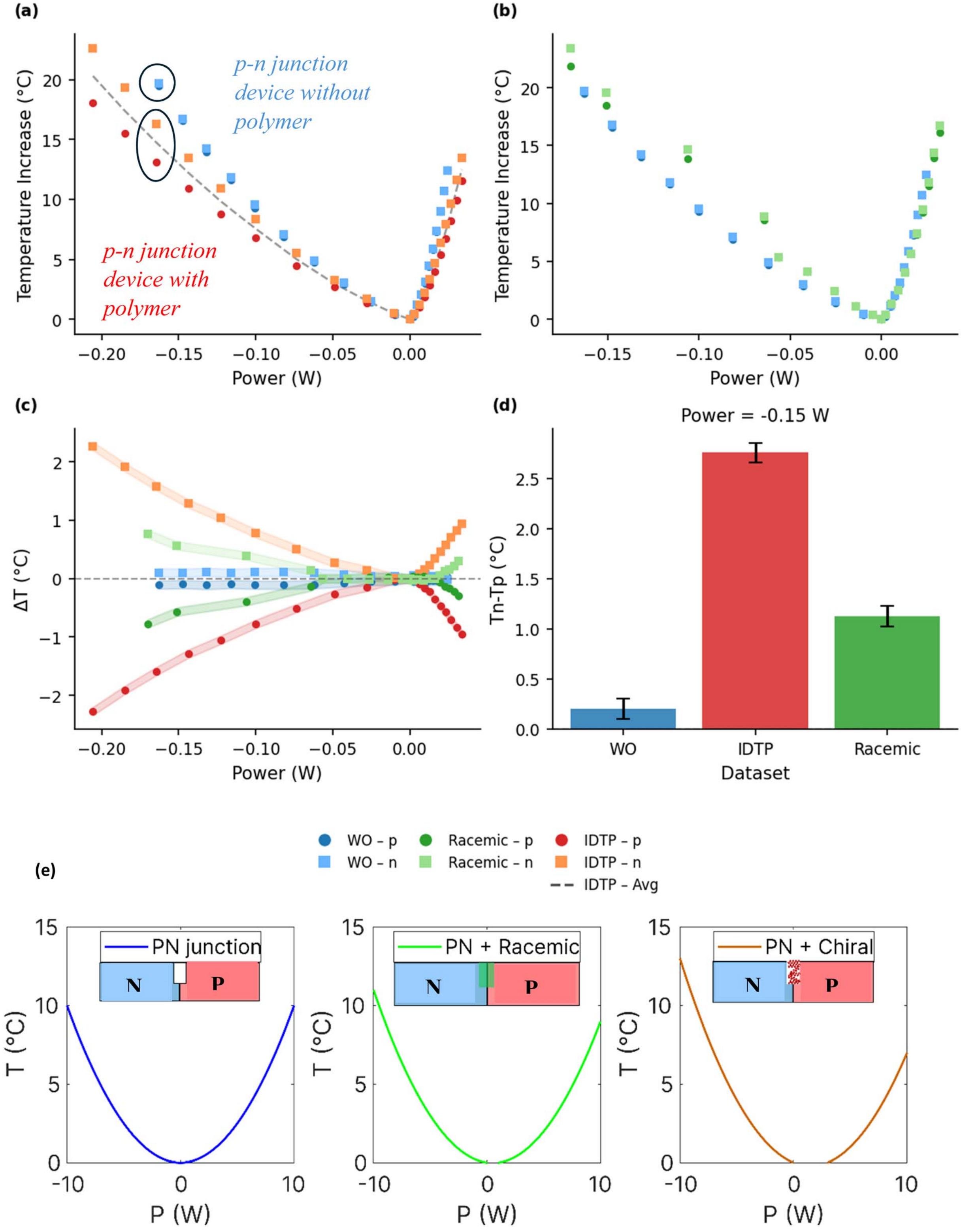

Fig. 4 (a and b) Comparison of the temperature change on the n and p sides of the device as a function of input power: power is defined as positive for forward current and negative for backward current in the p–n junction. (a) The p–n junction device without polymer (WO) *versus* after depositing the chiral polymer IDT-P, and (b) after depositing the racemic polymer mixture (Racemic) *vs.* IDT-P. Measurements. (c) The temperature difference between the p and n contacts scaled by the average device temperature for WO, IDT-P, and racemic, *i.e.*, $\Delta T = T_\mathrm{n} - T_\mathrm{avg}$ and $\Delta T = T_\mathrm{p} - T_\mathrm{avg}$, for each condition. (d) Interpolated temperature difference ($T_\mathrm{n} - T_\mathrm{p}$) at an input power of $P = -0.15$ W for the different conditions (see the circles in (a)). Depositing the chiral polymer significantly enhances the scaled temperature difference; at $P = -0.15$ W, the increase exceeds an order of magnitude compared with the bare device. The environmental temperature was controlled to be 22 ± 1 C. The total error bars were calculated as the geometric sum of the systematic instrument limit and the random temporal noise. (e) A schematic explanation

racemic polymer (Racemic), and with enantiopure *P*-IDT6-Hel polymer (IDT-P). The same p–n junctions were used for all measurements after removing the measured molecules, thus eliminating any differences in contact resistance. Note that the WO p–n device element is 200 nm thick, whereas the device elements for the Racemic and IDT-P have a 200 nm-thick p–n junction and a 100 nm-thick p–polymer–n junction in parallel. Electrical measurements on the different device structures exhibit clear diode-like behavior, with a notable asymmetry between forward and reverse bias, consistent with proper p–n junction functionality (SI Fig. S3 and 3a). In addition, a clear difference was noted in the temperature profile when adding the chiral polymer (Fig. 3b). For all device conditions, the overall temperature increased with applied electrical power because of Joule heating (Fig. 3b). The heating was asymmetric with respect to forward and reverse voltage bias, consistent with the diode-like electrical behavior of a p–n junction.

To compare cooling and heating using the same device with a different polymer, in Fig. 4 we plot the temperature difference between the p and n side of the junction as a function of injected power (for forward and backward bias). Even without any molecules placed in the top part of the junction, a temperature difference was observed between the p and n sides of the device, which is attributed to the Peltier effect arising from the bottom (100 nm thick) p–n junction (Fig. 4a–c). Notably, the temperature rise on the n-side (T_n) was consistently greater than on the p-side (T_p), such that $T_n > T_p$; *i.e.*, a gradient in the temperature profile exists. This temperature difference was significantly enhanced for the IDT-P devices, compared to both the racemic and WO devices, indicating a strong contribution of polymer chirality to the thermoelectric response.

Fig. 4c shows the temperature difference between the p and n contacts compared to the average temperature, which is colder; the polymer exhibits better heat transfer to the environment, $\Delta T = T - 1/2(T_n + T_p)$ with $T = T_n$ or $T = T_p$. The measurements were done on the same device for WO, IDT-P, and Racemic (Fig. 4c), alternating the power by changing the applied current. For example, interpolation at a power of -0.15 W shows that the temperature difference between the p and n sides ($T_n - T_p$) is more than tenfold higher with the chiral polymer than without it, and more than twofold higher than with the racemic mixture (Fig. 4d). The same trend was observed for the opposite enantiomer; this phenomenon was reproducible across multiple repetitions on the same device and was consistent across different devices (SI Fig. S5). Lastly, note that the temperature of the same device with the chiral layer was lower for an applied current.

According to the thermoelectric theory, a current flowing through a junction between materials with different Peltier coefficients Π_p, Π_n induces a heat exchange given by $Q = I(\Pi_p - \Pi_n)$.[25] Because of the contact resistances and Schottky barriers, the current flowing through these p–n junctions cause a temperature increase for both forward and reverse bias (Fig. 4b and e). Since the energy levels in p-type and n-type silicon differ, a small temperature difference across the junction manifests itself – (see Fig. 4c and d, which show the results at 0.15 W).

Compared to the same device without the polymer in the slit, the device with the polymer was colder, on average, showing better coupling to the environment. This cannot be ascribed only to heat absorption by the polymer, since the racemic mixture of the polymer did not show this effect (Fig. 4b). Even more pronounced is the temperature difference measured between the n and the p side of the same device with and without the polymer (highlighted by circles in Fig. 4a). Without the polymer (WO), the temperatures on the p and n sides were found to be nearly equal ($T_n \approx T_p$), within the accuracy of the measurements, indicating a symmetric heat distribution at steady state. With the chiral polymer a temperature gradient ($T_n > T_p$) manifests itself. This gradient suggests that a different mechanism contributes to the heat conduction for devices with the chiral layer. Note that the effect is large even when a large part of the current flows below and around the slit that includes the organic molecules. Reversing the current reverses the direction of heat transfer, causing the hot and cold sides to switch. In the racemic mixture, the domains of different chirality can form. Each of the domains acts as spin filters generating the chiral thermodynamic effect, whereas the border between domains acts as a mixer. Therefore, the racemic mixture of the polymers induces a small cooling effect.

In typical p–n junctions displaying the Peltier effect, the temperature difference reverses with bias polarity, yielding $T_n > T_p$ under forward bias and $T_p > T_n$ under reverse bias. This reversal is within our noise level without the polymer being present in the devices. With the polymer present, however, our devices have $T_n > T_p$ under both forward and reverse bias. This behavior was repeated in five devices. This effect can be attributed to the fact that entropy gain or loss is associated with the spin distribution of the electron current that is moving in the chiral media. In other chiral structures, fitting the current–voltage behavior for metal-chiral film-ferromagnet (M-χ-FM) structures display barrier differences of $\sim$100 meV,[26] much larger than K_BT at room temperature. The heating of the injecting contacts will occur when the unoccupied states in the lower spin band can be filled and emit a phonon, whereas cooling will occur if all these states are occupied, and phonons are absorbed to go to the upper spin state. Heat flow in the chiral case may also be better due to phonon scattering reduction (Fig. S6). Electrons (with the right spins) will emit phonons at the injecting contact as they fill empty states; in contrast, the injecting contact will cool down if states above the Fermi energy (see the Discussion section). Therefore, a flip is expected in the sign of the temperature gradient between forward and backwards current in this mechanism, compared with standard

of the results showing the temperature increase expected in the junction for each configuration. The heating of the junction due to contact resistance is generated by non-optimal contacts to the p–n-junction. Peltier adds a little to the thermal gradient and generates a small effect in the racemic mixture. Adding spin polarization induces a much larger effect and therefore a larger thermal gradient.

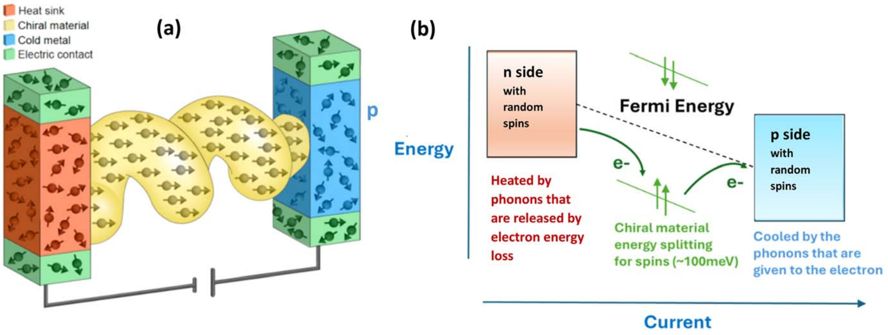

Fig. 5 A schematic of the spin thermoelectric effect in a magnetless device containing a chiral polymer. (a) For forward current the aligning spins cool down the p-side and warm up the n-side. (b) An energy scheme for the process.

Peltier. For the p–n junction without the polymer, the difference in temperature between sides for forward and reverse bias is very small, which indicates a small Peltier effect in this configuration, whereas a large difference was measured for the CISS cooling effect.

Discussion

The p–n junctions are not ideal; however, all the p–n junction devices display a Peltier effect arising from the bottom 100 nm part of the junction. Although its contribution to the overall thermal behavior is small, it must be considered in understanding the thermal profile. For the Peltier effect, the asymmetry in temperature on the two sides of the junction is small, since both contacts are placed on the same heat sink. In the device with no molecules, $T_n \approx T_p$, which means that the contact resistance, Joule heating, and recombination heating dominate the thermal behavior of the device.

The introduction of a polymer into the gap between the p and n sides causes a large increase in the temperature difference. Also, the chiral polymer significantly enhances the thermal response beyond that of the racemic polymer and increases the thermal gradient. Notably, the temperature increase on the n-side (T_n) is substantially greater than that on the p-side (T_p), such that $T_n > T_p$. This directional dependence indicates that the chiral polymer markedly enhances the effective Peltier coefficient, thereby improving the device's thermoelectric efficiency. For 0.15 W the temperature difference between the n-side and p-side of the junction was larger than 2.5 degrees Celsius for a non-insulated junction. These results highlight the significant impact of the chiral layer on the thermoelectric performance of the p–polymer–n device element.

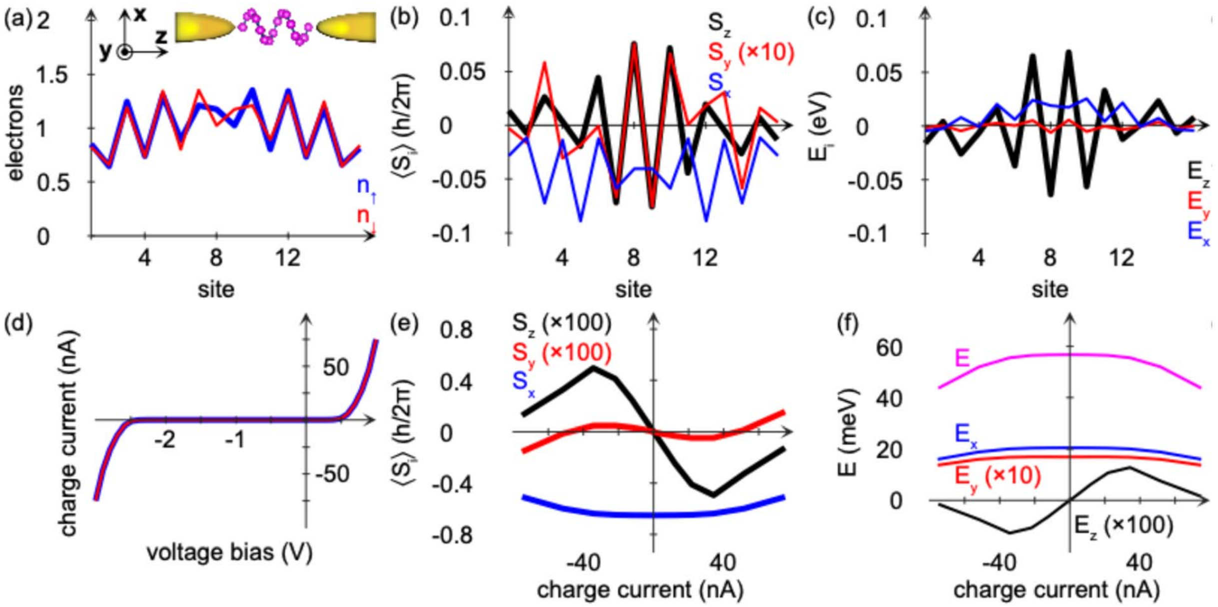

Fig. 6 (a) The site-resolved charge distribution of a 16-site helix wound around the z-axis in two laps (see the inset). (b) The corresponding site-resolved spin projections $\langle S_i \rangle$, $i = x, y, z$ and (c) spin-dependent energies E_i. (d) The charge current for (blue) chiral and (red) achiral molecules with 16 sites. (e) The corresponding total molecular spin moment as a function of the charge current, and (f) the energy associated with the spin formation.

The same trend was observed for the opposite chirality with temperature differences around 2 degrees Celsius.

The spin restriction arising from the chiral molecules is attributed to the chiral-induced spin selectivity (CISS) effect. As a result of the CISS effect, the transmission of electrons through the chiral layers is spin selective. When electrons enter the chiral system the two spin subsystems (parallel and anti-parallel to the electron momentum) experience different 'resistances' and energy barriers. For forward bias, the majority carriers consist of electrons injected from the n-side to the p-side. Here, when the chiral layer splits the spins, the charge carriers are injected and fill the spin hole states, releasing heat to the contact. This is shown in Fig. 5a and b. The spin alignment reduces energy, and heat is released at the n-side of the contact, whereas on the p-side, phonons are absorbed for the electrons to climb to the Fermi energy level in the contact. Injecting the current from the p-side under reverse bias reduces the total current, since the current is governed by the minority charge carriers and the spin injection is above the Fermi surface. Here, spin alignment occurs by taking energy from phonons on the p-side of contacts. Therefore, the p-side will be cooler, and the n-side will be warmer, as with the case of forward bias.

In our theoretical model we claim that the temperature gradient emerging in the n–chiral–p junction is attributed to the formation of molecular spin configurations. This interpretation is based on theoretical modeling showing that chiral molecules acquire a chirality-protected spin configuration when interfaced with a reservoir.[27] In the modeled scenario, the reservoir is represented by the p- and n-doped sides of the junction to which the chiral molecule may lose charge and energy, as well as linear and angular momentum to stabilize the spin orientation. Fig. 6a shows a site-resolved chiral charge distribution that is projected onto spin up (blue) and spin down (red) components for a helical molecule with 16 sites wound around the z-axis in two laps (see the inset). The charge distribution is locally spin-polarized throughout the molecule, an effect caused by the confluence of inelastic scattering among the correlated electrons and the leakage to the reservoir. The full molecular spin distribution is plotted in Fig. 6b, showing that the spins are arranged in a non-collinear distribution.

The formation of the local spin distribution is associated with renormalization of the energy spectrum. The product between the effective spin–orbit coupling and the density of the electron states of the reservoir causes a local Zeeman-like spin-splitting of the molecular energy spectrum. In Fig. 6c, the resulting spin-dependent energies projected onto the molecular sites are plotted, corresponding to the spin distribution in Fig. 6b. The spin-splitting of the energy levels is nearly as large as 75 meV in the example, an energy that is ultimately exchanged with the reservoir. This large energy splitting is the source for the large effect measured.

Although the plots in Fig. 6a–c are calculated for zero voltage bias, both the spin and energy distributions are expected to vary with the current flux through the junction. In Fig. 6d, the charge current is plotted as a function of the voltage bias, reproducing the p–n junction characteristics. The corresponding changes to the total molecular spin moment and the associated formation energy are plotted in Fig. 6e and f, as a function of the charge current. Clearly, a non-trivial total spin moment is manifested for all currents; whereas the S_x-projection decreases with increasing current amplitude, the S_y- and S_z-projections go from being extremely small (almost vanishing) to becoming non-zero. These changes in the total molecular spin moment under current, particularly the S_z-projection, signifies that the non-equilibrium conditions facilitate a non-vanishing spin imbalance. The generation of this spin imbalance is directly related to changes in the total spin formation energy; however, see Fig. 6f. This energy must be absorbed in the source reservoir and subsequently deposited in the drain where the transported electrons randomize their spins.

Summary

The novel phenomenon reported here is similar to both the Peltier and the magneto-cooling effects.[12,13] Regarding magneto-cooling, the temperature drop results from adiabatic demagnetization of a ferromagnetic material. Because electron transmission through chiral systems depends on their spin, the spin current produces a temperature gradient so that the source becomes hotter and the drain becomes colder. This effect can be viewed as the inverse of the chiral-phonon-activated spin Seebeck (CPASS) effect,[17] in which a spin current is induced in a chiral system by creating a temperature gradient between its two ends.

Chiral cooling draws conceptual parallels with two well-established thermoelectric phenomena. In the Peltier effect, a temperature gradient emerges at the junction of dissimilar conductors when current flows. In magnetocaloric cooling, entropy is modulated through the magnetization and demagnetization of a material. Chiral cooling unifies both principles through the interplay of electron spin and structural chirality. The flow of spins generates a spin Peltier effect, whereas the organization of the spin without an external field enhances the effect through an entropy change in the contact regimes.

It is important to note that the measured effect mixes p–n Peltier effect together with chiral phonon, heat flow and spin alignment. Future studies should address each component separately by theory and experiments. For example, measuring the effect without a p–n junction at different temperatures following by temperature dependence theory.

The total change in resistance when adding the polymer is small. Assuming parallel conduction channels, less than 50% of the current passes through the polymer, whereas most of the current passes around the junction. This behavior arises from the structure of the device, as well as the lower conductivity of the polymer. If the observed effect is scaled to account for this feature, then one finds that a fivefold enhancement of the cooling effect results from using enantiopure chiral molecules, which implies that the cooling effect observed here is larger than the Peltier effect by an order of magnitude.

Conflicts of interest

There are no conflicts to declare.

Data availability

All data generated or analyzed during this study are included in this published article [and its supplementary information (SI)]. Supplementary information: additional data and results including process description. See DOI: https://doi.org/10.1039/d6ta01920j.

Acknowledgements

The European Commission Research Executive Agency (Grant Agreement Number 859752 – HEL4CHIROLED – H2020-MSCA-ITN-2019) is thanked for financial support. J. C. acknowledges the Centre National de la Recherche Scientifique (CNRS), and the University of Rennes. C. L. C. acknowledges the Hellenic Foundation for Research and Innovation (H.F.R.I.) under the "2nd Call for H.F.R.I. Research Projects to support Faculty Members & Researchers" (Project Number: 4694). DHW acknowledges support from an NSF-BSF grant (CHE-2420811). YP and RN acknowledge the support of NSF-BSF grant (no. 2024621) and of US Airforce funding (no. FA8655-24-1-7390). YP also acknowledges the support of an ISF grant (no. 360/24).

References

1 A. Peterson, B. Perez and D. Zuckerman, *Envisioning a High Load Growth Future: Data Centers. Retrieved from the University Digital Conservancy*, 2025, https://hdl.handle.net/11299/272538.

2 See for example: J. R. Sootsman, D. Y. Chung and M. G. Kanatzidis, New and Old Concepts in Thermoelectric Materials, *Angew. Chem.*, 2009, **48**, 8616–8639.

3 M. K. Mahek, M. Ramadan, S. S. bin Dol, M. Ghazal and M. Alkhedher, A Comprehensive Review of Thermoelectric Cooling Technologies for Enhanced Thermal Management in Lithium-Ion Battery Systems, *Heliyon*, 2024, **10**(24), e40649.

4 G. J. Snyder and E. S. Toberer, Complex Thermoelectric Materials, *Nat. Mater.*, 2008, **7**(2), 105–114.

5 M. Goel and M. Thelakkat, Polymer Thermoelectrics: Opportunities and Challenges, *Macromolecules*, 2020, **53**(10), 3632–3642.

6 N. Kim, S. Lienemann, I. Petsagkourakis, D. Alemu Mengistie, S. Kee, T. Ederth, V. Gueskine, P. Leclère, R. Lazzaroni, X. Crispin and K. Tybrandt, Elastic Conducting Polymer Composites in Thermoelectric Modules, *Nat. Commun.*, 2020, **11**(1), 1424.

7 D. Brown, N. Fernandez, J. Dirks and T. Stout, *The Prospects of Alternatives to Vapor Compression Technology for Space Cooling and Food Refrigeration Applications*, US Department of Energy, 2010.

8 G. E. W. Bauer, E. Saitoh and B. J. van Wees, Spin caloritronics, *Nat. Mater.*, 2012, **11**, 391–399.

9 A. Hoffmann and S. D. Bader, Opportunities at the frontiers of spintronics, *Phys. Rev. Appl.*, 2015, **4**, 047001.

10 K. Uchida, *et al.*, Observation of the spin Seebeck effect, *Nature*, 2008, **455**, 778–781.

11 A. Slachter, F. L. Bakker, J. P. Adam and B. J. van Wees, Thermally driven spin injection from a ferromagnet into a non-magnetic metal, *Nat. Phys.*, 2010, **6**, 879–882.

12 K. Uchida, *et al.*, Long-range spin Seebeck effect and acoustic spin pumping, *Nat. Mater.*, 2011, **10**, 737–741.

13 J. Flipse, F. L. Bakker, A. Slachter, F. K. Dejene and B. J. van Wees, Direct observation of the spin-dependent Peltier effect, *Nat. Nanotechnol.*, 2012, **7**, 166–168.

14 C. M. Jaworski, R. C. Myers, E. Johnston-Halperin and J. P. Heremans, Giant spin Seebeck effect in a non-magnetic material, *Nature*, 2012, **487**, 210–213.

15 S. M. Wu, J. E. Pearson and A. Bhattacharya, Paramagnetic spin Seebeck effect, *Phys. Rev. Lett.*, 2015, **114**, 186602.

16 S. Meyer, *et al.*, Observation of the spin Nernst effect, *Nat. Mater.*, 2017, **16**, 977–981.

17 K. Kim, *et al.*, Chiral-phonon-activated spin Seebeck effect, *Nature Materials*, 2023, **22**, 322–328.

18 K. A. Gschneidner Jr, V. K. Pecharsky and A. O. Tsokol, Recent developments in magnetocaloric materials, *Rep. Prog. Phys.*, 2005, **68**, 1479–1539.

19 X. Tang, *et al.*, Magnetic refrigeration material operating at a full temperature range required for hydrogen liquefaction, *Nat. Commun.*, 2022, **13**, 1817.

20 A. Ziv, A. Saha, H. Alpern, N. Sukenik, L. T. Baczewski, S. Yochelis, M. Reches and Y. Paltiel, AFM-Based Spin-Exchange Microscopy Using Chiral Molecules, *Adv. Mater.*, 2019, **31**, 1904206.

21 B. P. Bloom, Y. Paltiel, R. Naaman and D. H. Waldeck, Chiral Induced Spin Selectivity, *Chem. Rev.*, 2024, **124**(4), 1950–1991.

22 C. Gedeon, *et al.*, Design of New Conjugated Polymers with Main Chain Chirality for Efficient Optoelectronic Devices: Carbo[6]Helicene and Indacenodithiophene Copolymers as Model Compounds, *Adv. Mater.*, 2024, **36**(25), 2314337.

23 T. Kumar Das, O. Marelly, S. Yochelis, Y. Paltiel, R. Naaman and J. Fransson, Long-Range Spin Transport in Chiral Gold, *Adv. Mater.*, 2025, **37**(34), 2506523.

24 C. Gedeon, *et al.*, Circularly Polarized Luminescence from Benzodithiophene and Indacenodithiophene Oligomers Alternated with Helicenes as Chiral Inducers, *ACS Appl. Opt. Mater.*, 2025, **3**(9), 2207–2220.

25 H. J. Goldsmid, *The Physics of Thermoelectric Energy Conversion*, Morgan & Claypool Publishers, 2017.

26 A. Ziv, *et al.*, AFM-Based Spin Exchange Microscopy Using Chiral Molecules, *Adv. Mater.*, 2019, **31**, 1904206.

27 J. Fransson, Breaking of Time-Reversal Symmetry and Onsager Reciprocity in Chiral Molecule Interfacd with an Environment, *APL Comput. Phys.*, 2026, **2**, 016111.